THE DAVID W. TAYLOR MODEL BASIN

UNITED STATES NAVY

EARLY AND ULTIMATE DAMAGE DUE TO UNDERWATER EXPLOSIONS AGAINST 10-INCH DIAPHRAGMS

BY G. E. HUDSON, Ph. D.

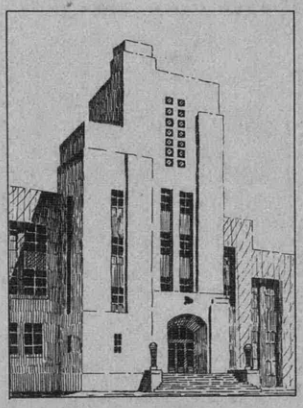

CONFIDENTIAL 48

AUGUST 1943

REPORT 509

NAVY DEPARTMENT
DAVID TAYLOR MODEL BASIN
WASHINGTON, D.C.

RESTRICTED

The contents of this report are not to be divulged or referred to in any publication. In the event information derived from this report is passed on to officer or civilian personnel, the source should not be revealed.

CONFIDENTIAL

REPORT 509

EARLY AND ULTIMATE DAMAGE DUE TO UNDERWATER EXPLOSIONS AGAINST 10-INCH DIAPHRAGMS

BY G. E. HUDSON, Ph. D.

AUGUST 1943

PERSONNEL

The data on which this report is based are the result of experiments carried out by C.T. Johnson with the assistance of W.P. Gleason and under the direction of G.E. Hudson. The report was written by G.E. Hudson.

DIGEST

The pressure-time phenomenon for the initial stages of an explosion in free water may be represented by the diagram of Figure 1, in which an almost instantaneous rise in pressure accompanying the shock front is followed by a more or less exponential decay in pressure. This initial pulse, lasting until the pressure has decreased to about 20 per cent of the maximum, is called the A-phase. Following it is the B-phase, in which there is reason to believe that a fairly steady pressure exists for a time that is relatively long compared to the A-phase, but still short compared to the period of the first oscillation of the gas globe.

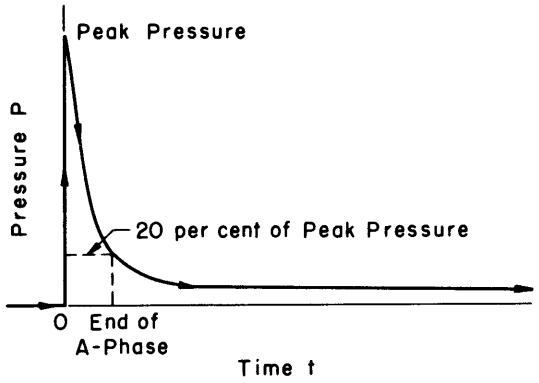

Figure 1 - A Typical Free-Field Pressure Record of a Shock Wave from an Underwater Explosion

There is definite evidence that a target placed in the field of an underwater explosion may be damaged, not only during the A- and B-phases, but at a later time. Pressures causing these latter effects are lumped together in this report under the title of C-phase phenomena, and they include pressures due to the pulsations of the gas globe following the A- and B-phases.

The main purpose of this report is to present indirect but striking evidence for the existence of C-phase pressures. The data obtained from these experiments point to the conclusion that when a charge is within a certain range of distances from a target, by far the major portion of the damage is done by some action other and later than that of the initial shock wave.

The model structures which served as targets in this series of experiments were thin circular diaphragms of furniture steel 10 inches in diameter and 0.057 inch thick. They were welded around the periphery to a heavy ring which was in turn clamped to a mount in the bottom of a flat-bottomed steel barge floating freely in the water. The charges were 3/4 ounce of tetryl, fired directly under the center of the diaphragms. The only variable was the vertical distance from the charge to the diaphragm; this covered a range from 18.5 to 24 inches, with tests on 10 diaphragms.

At 20 inches distance in free water, the A-phase of the charge, with a peak pressure of 3600 pounds per square inch, ends in about 0.031

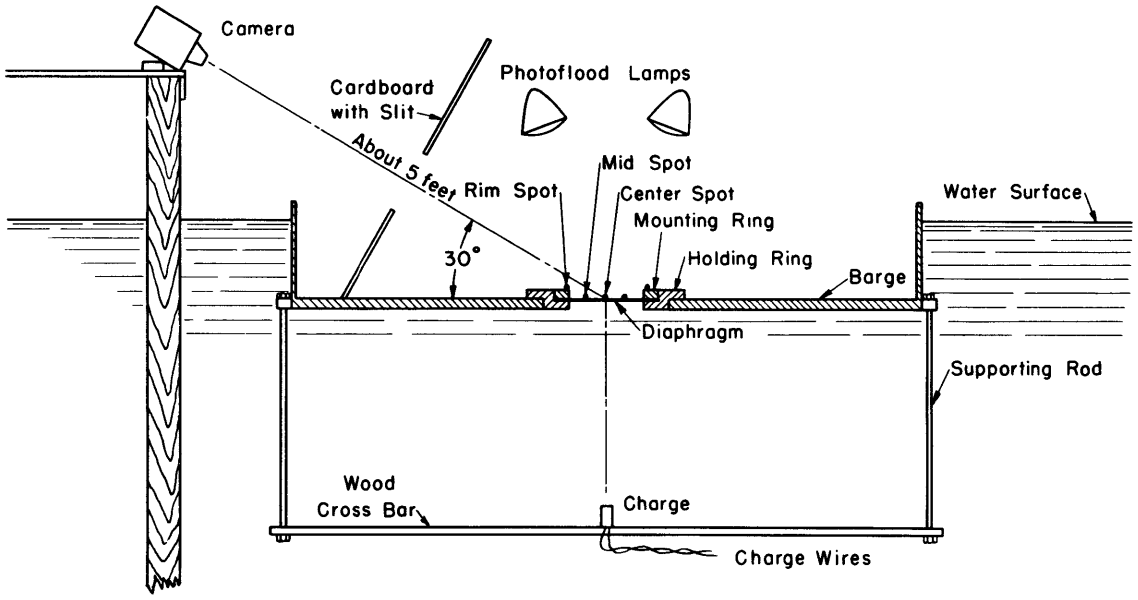

Figure 7 - Arrangement of Apparatus for obtaining Streak Photographs

millisecond, whereas the B-phase is estimated to continue for about 1 or 1.5 millisecond. The gas globe from a charge of this size undergoes its first compression 75 milliseconds after the explosion. A second pressure pulse is sent out at this time and possibly constitutes the first part of the C-phase.

The apparatus was set up to obtain streak photographs as shown in Figure 7. The diaphragm was painted black and on its surface there were mounted three shiny steel balls, or there were painted three small spots of aluminum, to serve as light reflectors.

The record made on a continuous strip of film is represented by the typical diagram of Figure 8, which shows an extremely abrupt change in direction of the lines at the instant of arrival of the first shock wave, representing an extremely high acceleration.

A plot of the deflection-time data for the streak photographs of the diaphragms tested indicates that the successive phases of deformation of

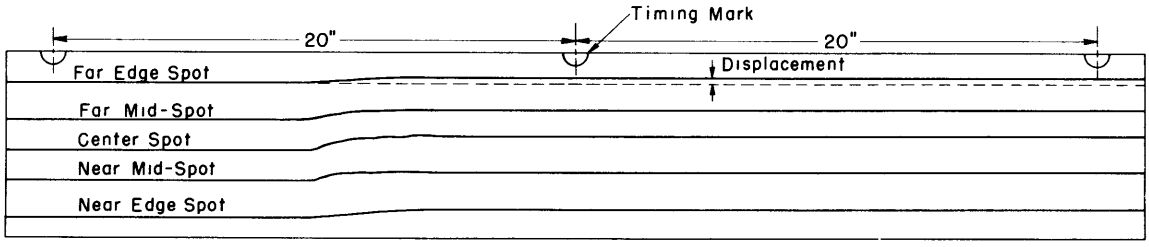

Figure 8 - Diagram of a Streak Photograph

In this case the far edge and near edge spots are on the mounting ring, and their position serves as a reference base from which the diaphragm deflection was measured.

the diaphragm under explosive load are about as shown in the diagram of Figure 14. In the first motion, a more or less fixed slope is assumed just inside the boundary. The center portion of the diaphragm remains quite flat but it decreases in area as the deformation progresses.

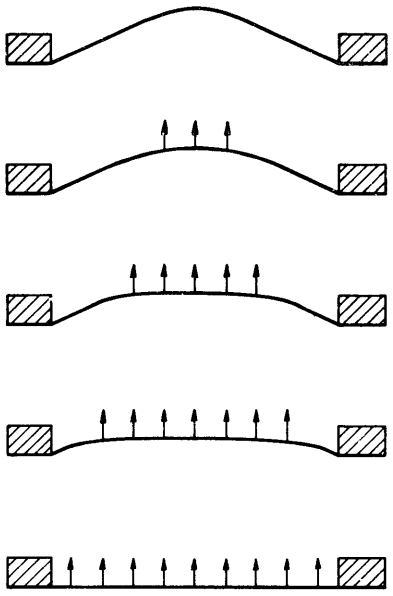

Figure 14 - Motion of the Diaphragm Inferred from the Streak Photographs

The time scale reads from the bottom upward. The arrows indicate motion of the diaphragm.

The test results are set down and analyzed in a variety of ways in the report, on pages 16 to 24 inclusive. Of particular interest is Table 4 on page 17, which shows that whereas the ratio of ***final*** increase in area of the diaphragm to the increase in area at the end of its first maximum deflection is only about 1.8 at a charge distance of 24 inches, when the charge is moved in to 18.5 inches, this ratio increases to 18.8, ten times as large. In other words, if the charge is not too close, most of the damage to the diaphragm is done in the A- and B-phases, but if the charge is fired at less than a certain critical distance, the damage produced in the C-phase may be many times that which takes place in the combined A- and B-phases.

The greater part of the analysis is based upon a determination of the respective energy relations, which are used as a measure of the damage. Figure 13 shows again, in perhaps more striking fashion, the greatly increased damage occurring in the C-phase as the charge is moved nearer to the target.

Under the conditions and circumstances described in this report, we may state the following:

(a) Most of the damage done by an underwater explosion to a thin circular diaphragm, at less than a critical distance, occurs ***after*** the initial shock wave has ceased to act. This is evidence for the effectiveness of the C-phase in producing damage.

(b) At about 1.5 millisecond for a 22.7 gram charge, after which time both the A- and B-phase of the shock wave have passed, the damage to the diaphragm is less than if all the kinetic energy initially acquired had been

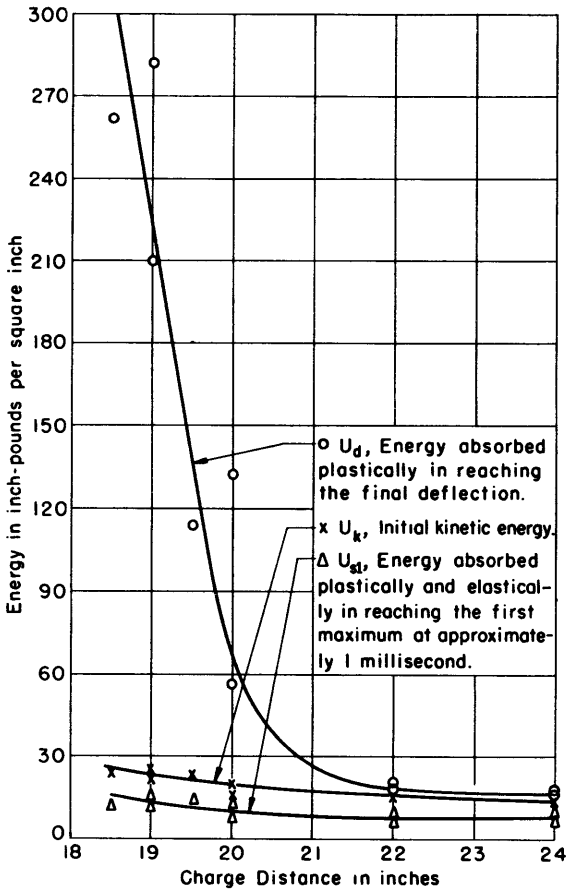

Figure 13 - Relation of Final to Initial Damages plotted from Table 6

expended in damaging the diaphragm. This is evidence against the effectiveness of the B-phase in causing damage.

(c) In the moderate range of charge distances investigated here the initial kinetic energy imparted by the initial shock wave to the target is roughly proportional to the solid angle subtended by the target at the charge.

The magnitudes of these effects for charges and diaphragms of different sizes have not yet been investigated. Experiments along these lines, together with an extension of the observations to larger ranges of charge distances, are planned for the immediate future.

EARLY AND ULTIMATE DAMAGE DUE TO UNDERWATER EXPLOSIONS AGAINST 10-INCH DIAPHRAGMS

ABSTRACT

In underwater explosion tests on a series of 10-inch diaphragms attacked by 22.7 grams of tetryl at various distances, it is demonstrated that as the distance between the charge and the diaphragm target diminishes, the damage increases very greatly as the charge is moved closer than 20 inches. It is also demonstrated that this increase cannot be caused by the initial shock wave. The inference is that in targets attacked by charges of this scale the later phases of the explosive action cause a large part of the damage.

INTRODUCTION

The separation and study of the significant variables governing the amount of damage produced by underwater explosions is one of the main objectives in the program being carried on by the David Taylor Model Basin for the protection of ship structures against underwater explosion. The particular investigation described in this report was designed to determine the relative effectiveness of successive explosion pressure phases in producing damage.

The usual pressure-time records in free water for an explosive such as tetryl show an initial steep rise, which occurs almost instantaneously compared with later portions of the record. This rise is associated with the initial shock front. Following this shock front, the pressure decays somewhat exponentially. This initial pressure pulse, followed down to about 20 per cent of its peak value, may be called the A-phase. The existence of a B-phase, a fairly steady pressure of relatively long duration following the A-phase pressure, has been postulated for some time; experimental evidence for or against it is still uncertain. Figure 1 is a typical pressure-time record of a shock wave in free water. This is based on typical records obtained at the Taylor Model Basin.

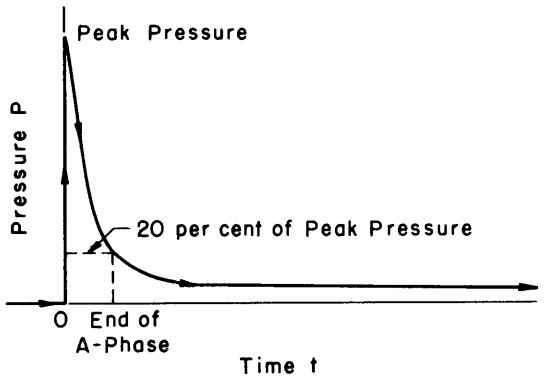

Figure 1 - A Typical Free-Field Pressure Record of a Shock Wave from an Underwater Explosion

The interaction of a target with the field of an explosion alters the characteristics of the free-field pressure-time record. For instance, when the shock wave impinges on a solid obstacle, the pressure is momentarily increased

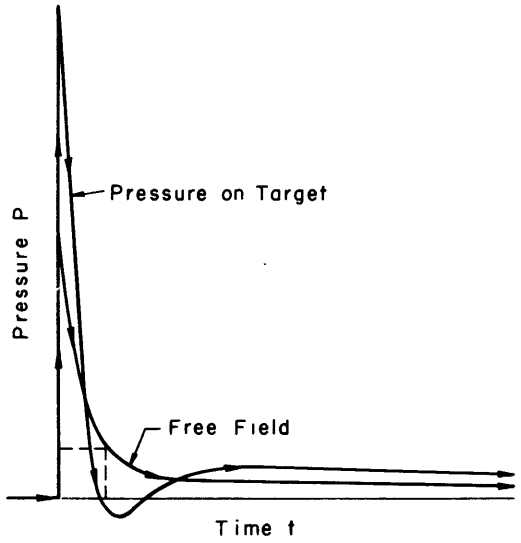

Figure 2 - Comparison of a Free-Field Pressure Record with the Pressure on a Movable Target

by a factor which may be as large as 2, depending on the density of the object. If the target is readily mobile so that it quickly attains a high velocity, this pressure falls off more rapidly than otherwise, even sinking to negative values if the water can withstand tension. The pressure is further modified by the shape and condition of support of the target. A possible pressure-time curve is compared with a free-field record in Figure 2.

A further modification may be produced in the shock wave pressure record if cavitation occurs in the tension phase of Figure 2. If this happens, the pressure immediately becomes zero, remaining so until the cavitation region disappears and later pressures come into play. A few indications of effects such as these are suggested by consideration of the data presented here.

There is definite evidence of the existence of damaging actions under certain conditions occurring later than either the A- or B-phases (1).* Pressures causing these effects may be lumped together for the present under the title "C-phase," including pressures due to the subsequent pulsations of the explosion gas globe.

The main purpose of this report is to present indirect but striking evidence for the existence of C-phase pressures. The data obtained from these experiments point to the conclusion that when the charge is within a certain range of distances from the model structure, by far the major portion of the damage is done by some action other and later than that of the initial shock wave.

TEST APPARATUS

MODEL STRUCTURES

The model structures which served as targets in these tests consisted of circular furniture steel** diaphragms 10 inches in diameter and

---

* Numbers in parentheses indicate references on page 25 of this report.

** This is a product used for automobile bodies and metal furniture, composed of almost pure iron with about 0.05 C, 0.02 Si, 0.36 Mn and small amounts of S, P, and Cu. It is rolled and then stretcher-leveled to obtain flatness. When so treated, it has a yield strength of about 44,000, an ultimate strength of about 52,500 and an elastic modulus of 29,000,000 pounds per square inch.

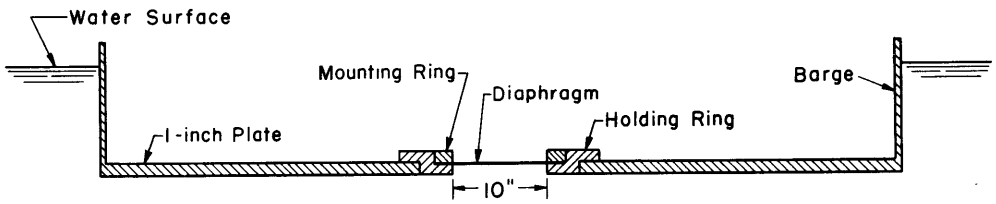

Figure 3 - Cross Section of the Barge and Diaphragm Mounting

0.057 inch thick. These were arc welded around the periphery to steel mounting rings 1 inch thick. Each diaphragm and ring was bolted in turn to a heavy steel holding ring in the flat bottom of a heavy barge. The barge was built of steel plate, 5 feet wide by 5.5 feet long. A 1-inch steel plate served as its bottom, and steel plates 1/4 inch thick, about 10 inches deep, served as its sides; see Figure 3. The whole assembly weighed approximately 1400 pounds and floated freely in the water during each test.

EXPLOSIVE CHARGES

The charges consisted of 22 grams (about 3/4 ounce) of tetryl in cylindrical bakelite containers. They were detonated by Number 8 caps* containing 0.42 grams of tetryl and 0.29 grams of other explosive. The shape and dimensions of the charge and detonator are shown in Figure 4.

At 20 inches distance in free water, the A-phase of such a charge, with a peak pressure of 3600 pounds per square inch, ends in about 0.031 millisecond, whereas the B-phase is estimated to continue for about 1 or 1.5 millisecond. The gas globe from a charge of this size undergoes its first compression 75 milliseconds after the explosion. A second pressure pulse is sent out at this time and possibly constitutes the first part of the C-phase.

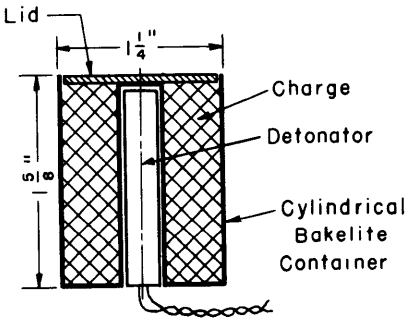

Figure 4 - The Charge and Container

As shown in Figure 5, the charge was mounted below the diaphragm and barge on a wood crossbar about 3/4 by 3/4 inch in cross section. The axis of the charge cylinder was carefully lined up to be coincident with the axis of symmetry of

---

* The composition of these caps is as follows:

Tetryl			0.42 gram
Lead Azide			0.16 gram
Mixture:	"Pyro"	0.07	
	Potassium Chlorate	0.03	
	Lead Salt	0.03	
			0.13 gram
Total			0.71 gram

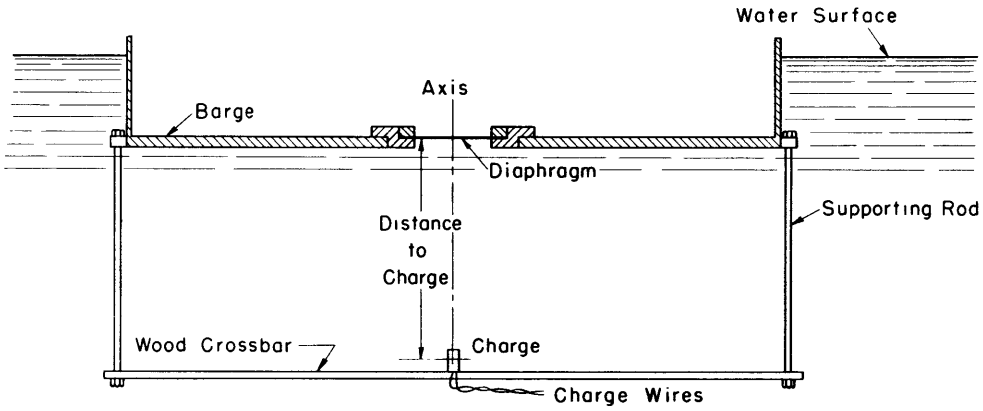

Figure 5 - The Charge Mount

the diaphragm. It was so directed that the end of the cylindrical container from which the detonator wires issued was facing away from the diaphragm. The only dimension which was varied throughout the experiment was the distance from the center of the charge to the center of the diaphragm.

STREAK PHOTOGRAPH TECHNIQUE

The top surfaces of four of the diaphragms, carrying the identification I-15, J-1, J-2, and J-3, were painted black after three 1/8-inch bearing balls had been welded to each of them. These balls were located on a diameter, one at the center and two midway between the center and the edge on opposite sides of the center. Because of the undesirable heating of the metal diaphragm surfaces by the welds, and because the balls frequently came off during the deformation, this technique was changed. On the next six diaphragms, J-5, J-6, J-7, J-8, J-9, and J-10, small rectangular spots of aluminum paint, approximately 1/16 inch by 1/8 inch, were applied to the black top surfaces of these diaphragms in place of the balls.

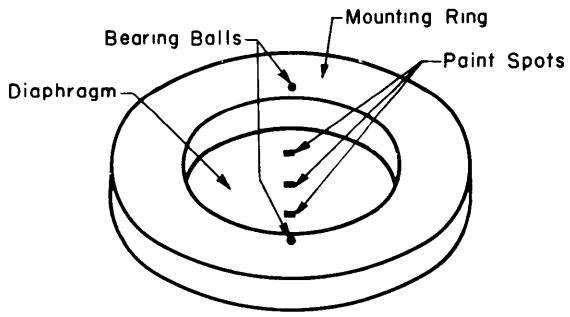

Figure 6 - Diaphragm and Holding Ring

The paint spots are indicated on the diaphragm. The bearing balls are mounted on the holding ring.

In both cases, two bearing balls were located on the mounting ring about 1/2 inch from the edge of the diaphragm, near the opposite extremities of the diameter through the three diaphragm spots, to serve as reference points on the mounting ring. Figure 6 is a sketch of a diaphragm and its mounting ring, with the location of the spots as seen from the point of view of the camera.

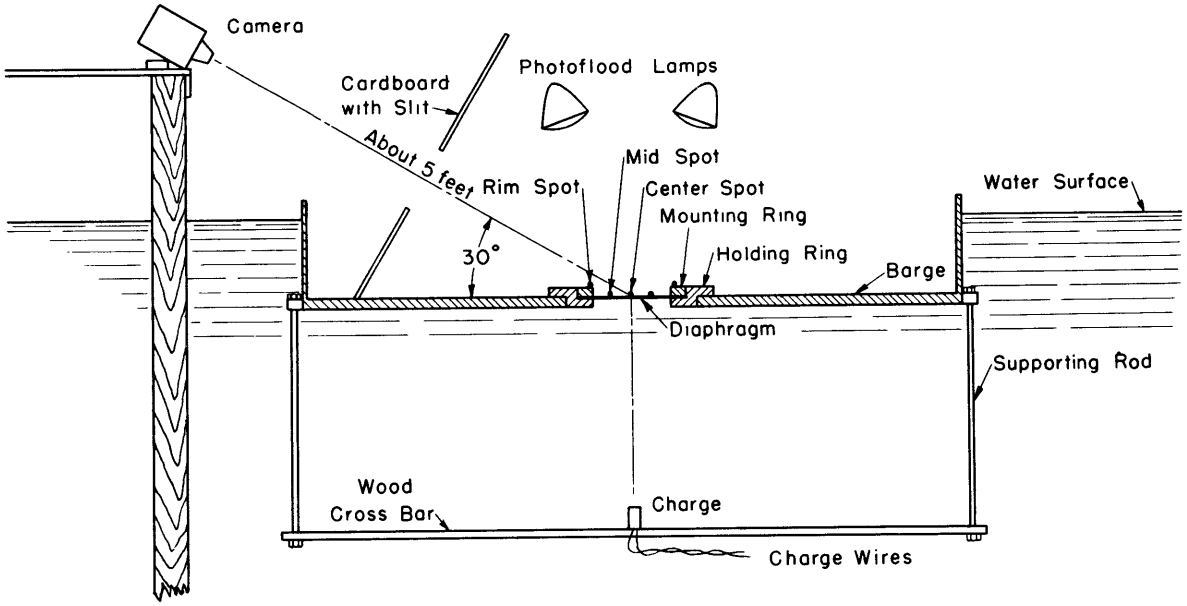

Figure 7 - Arrangement of Apparatus for obtaining Streak Photographs

The spots were illuminated with Number 2 photoflood bulbs; light was scattered from the paint spots and specularly reflected from the polished balls into the camera lens through a slit in a cardboard placed between the diaphragm and camera to exclude extraneous light. The camera itself stood on a platform built out over the basin in which the barge floated. Its optical axis was centered on the diaphragm, inclined at about 30 degrees from the horizontal, and lay in the vertical plane including the line through the five spots. The arrangement of the apparatus is shown schematically in Figure 7.

The camera used was a General Radio Camera with a Zeiss lens, focal length 6.5 inches. It was adjusted so that the film could run continuously. Moreover, the camera was fitted up with a Strobotac timing spark which made a small spot on the edge of the film at intervals of 1/60 of a second; see Figure 8. A mechanical relay attached to the camera tripped when the film

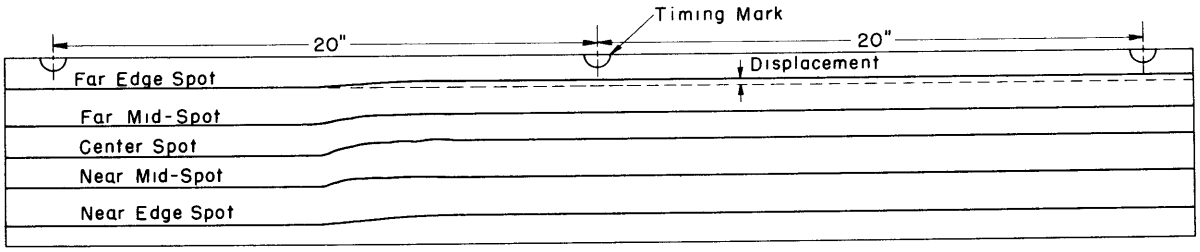

Figure 8 - Diagram of a Streak Photograph

In this case the far edge and near edge spots are on the mounting ring, and their position serves as a reference base from which the diaphragm deflection was measured.

was at the desired speed and set off the detonator. The diaphragm would then deform, and the spots and bearings would leave their characteristic streak records on the film.

The streak photographs thus made (2) have the appearance of fine continuous lines which depart from a straight line when deformation takes place, as indicated in Figure 8.

TEST PROCEDURE

As stated previously, the only dimension varied throughout the experiment was the distance between the charge and the diaphragm. A charge was mounted at a fixed distance in the range from 18.5 to 24 inches with the barge hoisted clear of the water. The barge was then lowered to the surface of the water, and the diaphragm and ring were bolted into position. Extreme care was taken to remove *all* bubbles from the under surface of the diaphragm, so that water was in direct contact with its entire surface. Finally, the whole assembly was lowered until it was just afloat.

After the camera lens had been focused approximately on the center spot about 5 feet distant, the timing spark was started, and then the camera. At the instant of each explosion, the film speed was approximately 1200 inches per second but not quite uniform, because of the short interval available for bringing it up to speed. Measurements indicated an almost constant acceleration of 630 inches per second per second at this point. Over the interval of interest, about 2 inches of film, the variation of speed because of this acceleration is at most 0.1 per cent. Consequently, if the acceleration is neglected in measuring the time scale on the film, the error produced is only about 0.05 per cent, which is well within the limits of error of the experiment.

Photographs of the ten diaphragms deformed by the explosion are shown in Figure 9 and the ten streak records in Figure 12 of the next section.

(Text continued on page 12)

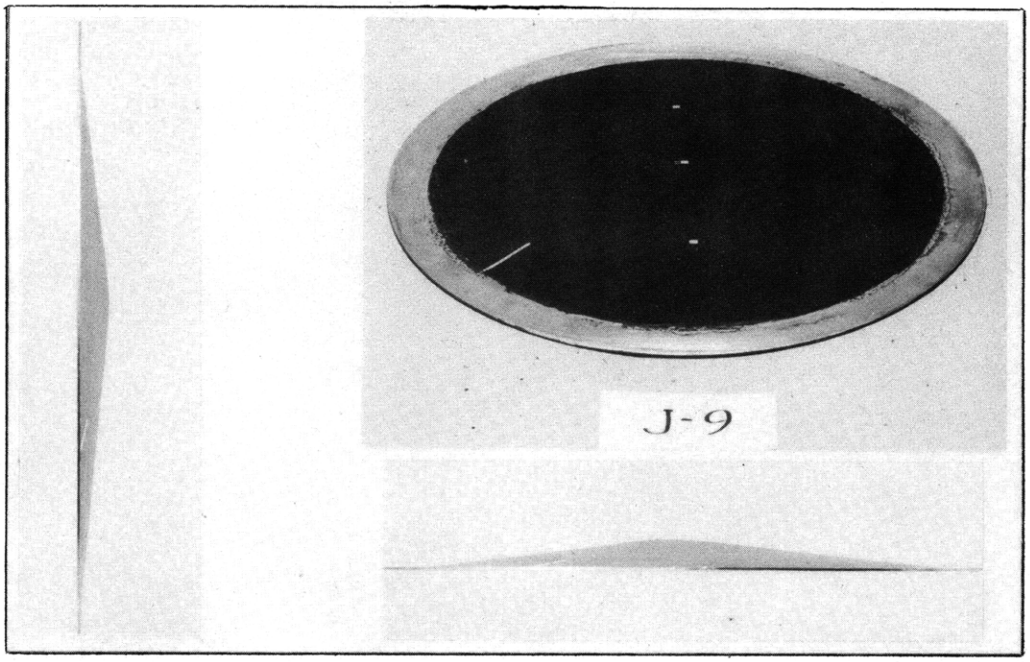

Figure 9a - Charge Distance 24 inches
The three paint marks are clearly visible.

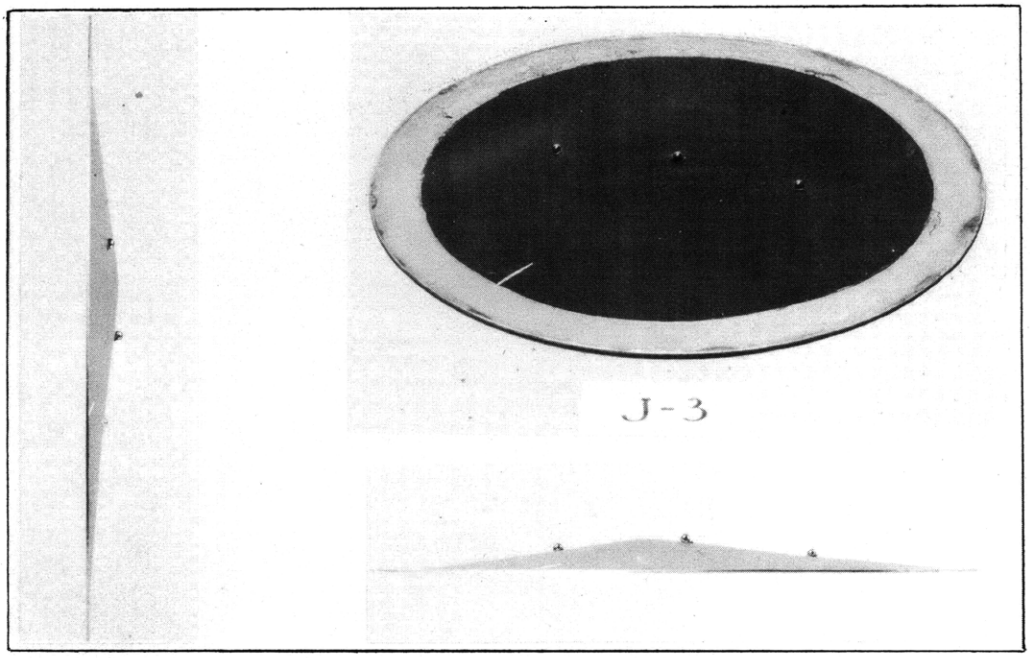

Figure 9b - Charge Distance 24 inches
The three projections are the three steel balls welded to the diaphragm.

Figure 9 - Photographs of Deformed Diaphragms, about 1/3 Actual Size

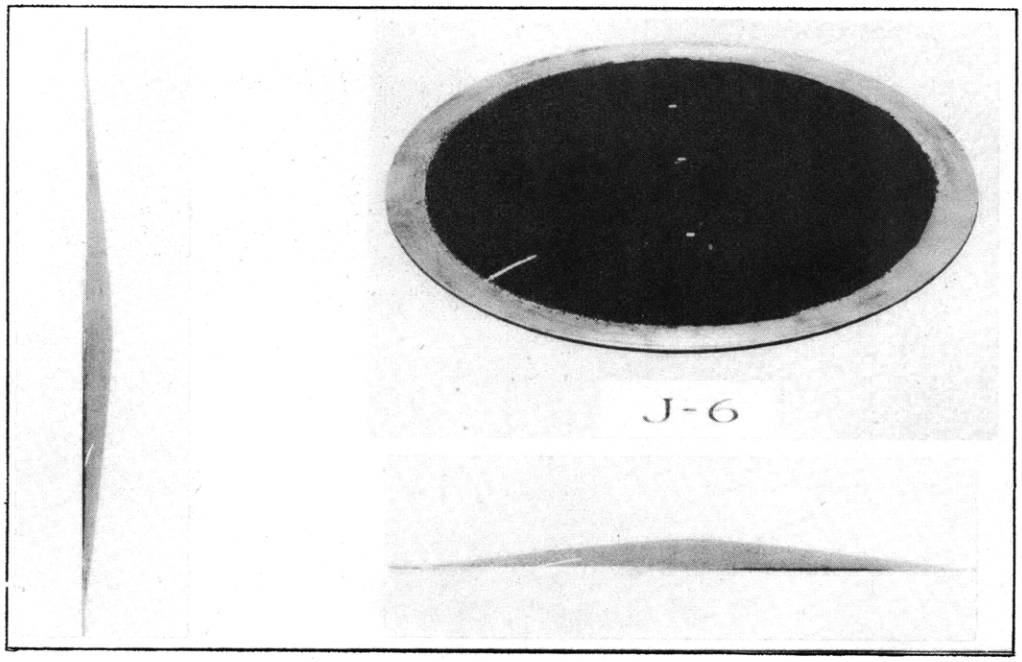

Figure 9c - Charge Distance 22 inches

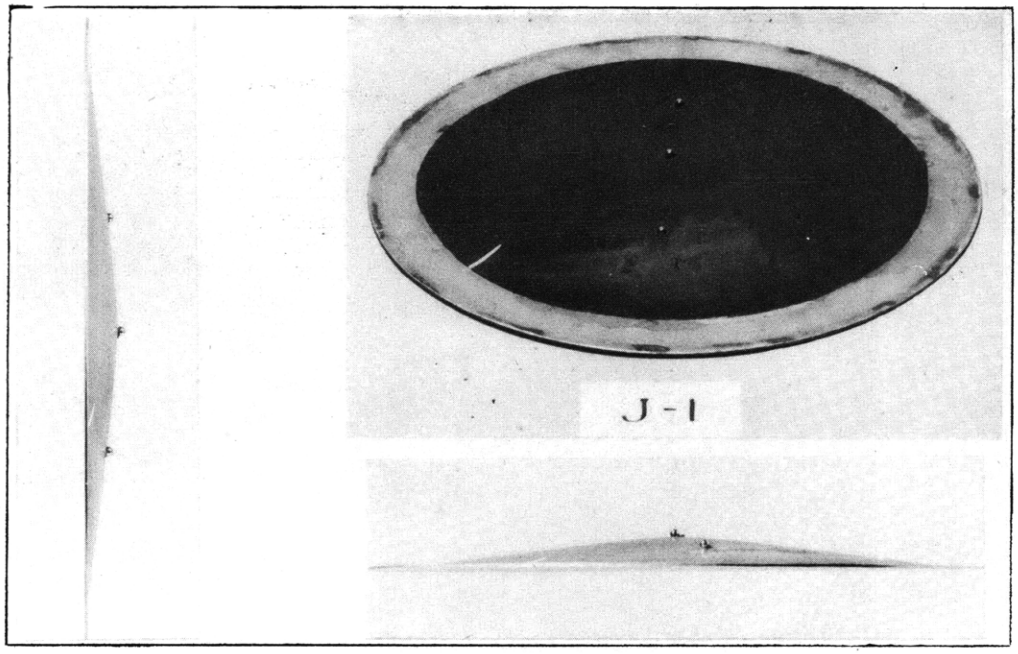

Figure 9d - Charge Distance 22 inches

Figure 9 - Photographs of Deformed Diaphragms, about 1/3 Actual Size

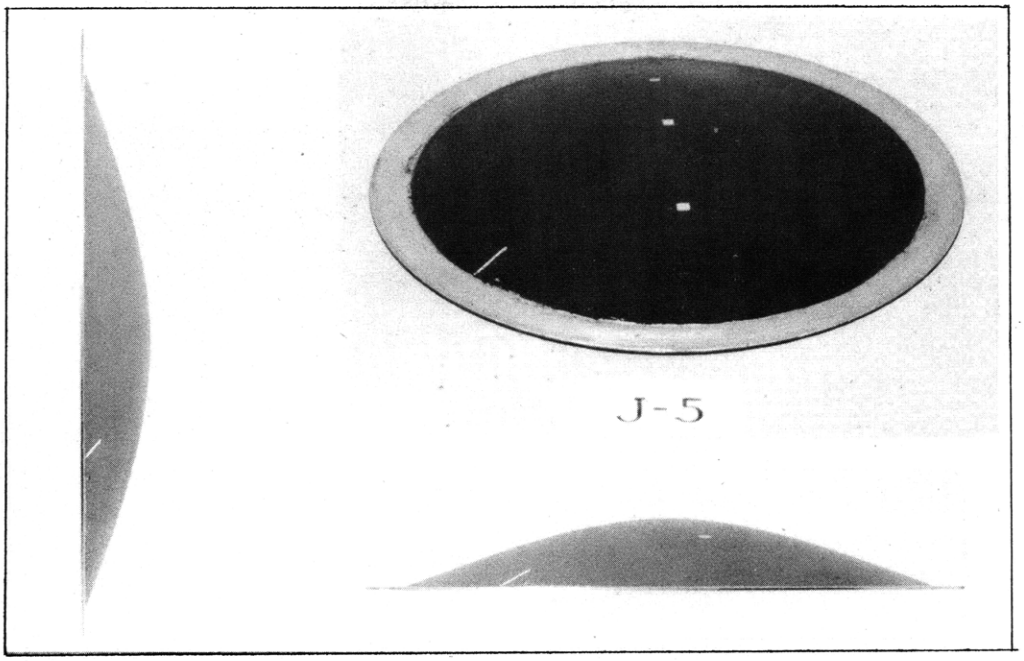

Figure 9e - Charge Distance 20 inches

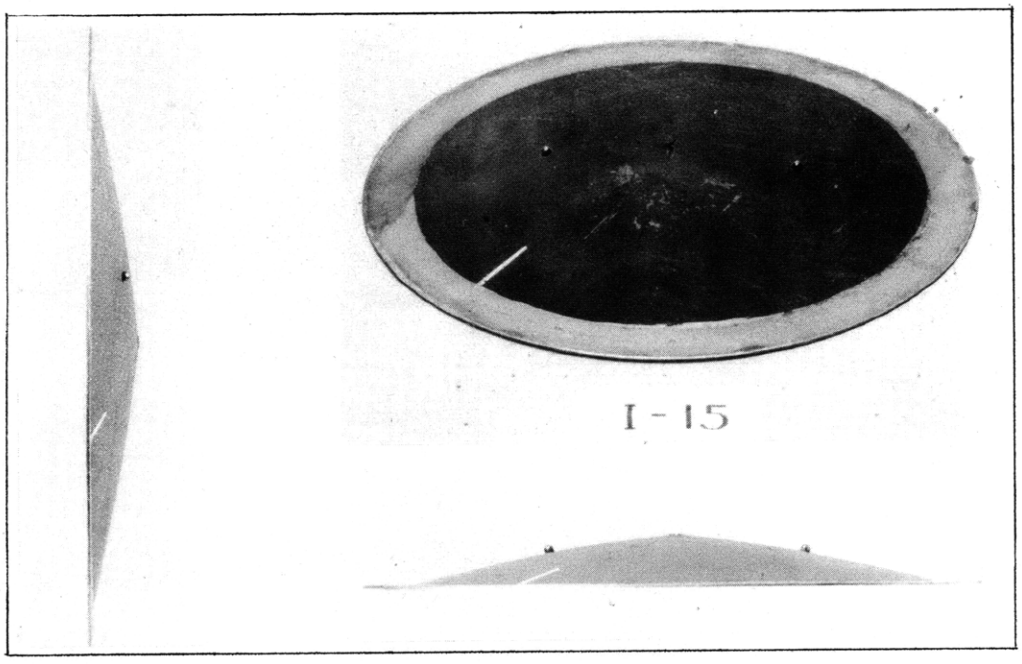

Figure 9f - Charge Distance 20 inches

Figure 9 - Photographs of Deformed Diaphragms, about 1/3 Actual Size

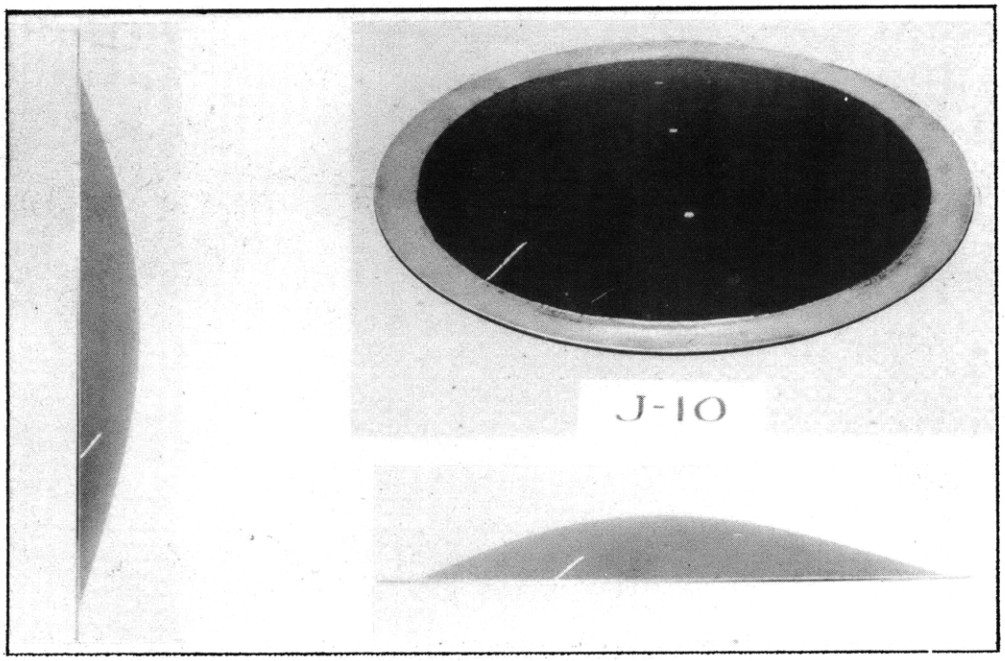

Figure 9g - Charge Distance 19.5 inches

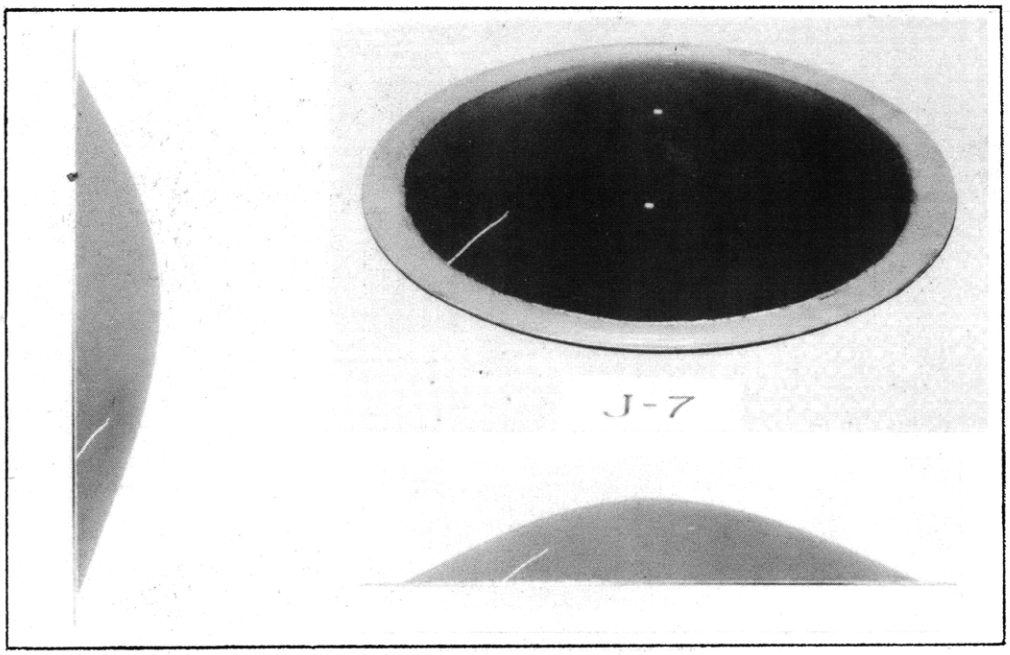

Figure 9 - Photographs of Deformed Diaphragms, about 1/3 Actual Size

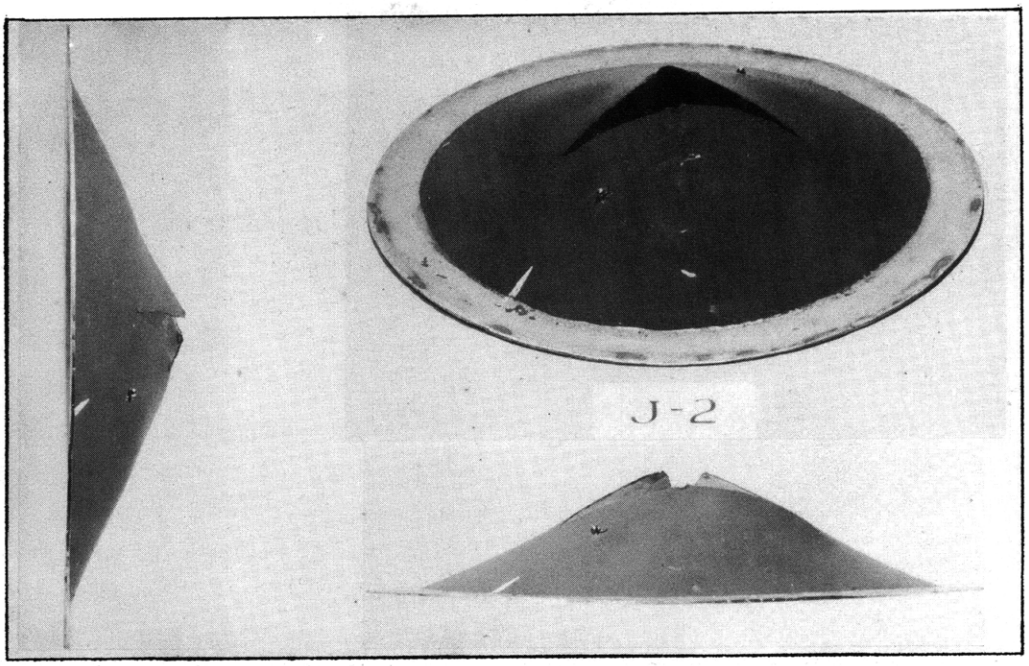

Figure 9i - Charge Distance 19 inches

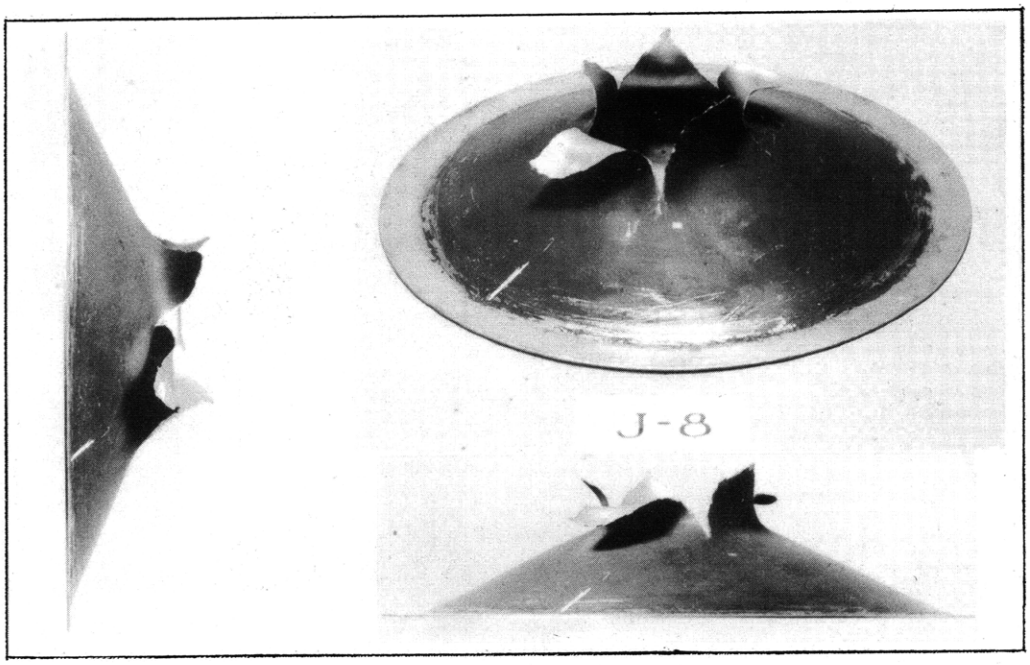

Figure 9j - Charge Distance 18.5 inches

Figure 9 - Photographs of Deformed Diaphragms, about 1/3 Actual Size

TABLE 1

Distances between Charges and Targets

Diaphragm	Type of Spot	Charge Distance inches
J-9	Paint	24.0
J-3	Ball	24.0
J-6	Paint	22.0
J-1	Ball	22.0
J-5	Paint	20.0
I-15 (R)*	Ball	20.0
J-10	Paint	19.5
J-7	Paint	19.0
J-2 (R)	Ball	19.0
J-8 (R)	Paint	18.5

* (R) indicates that the diaphragm was eventually ruptured.

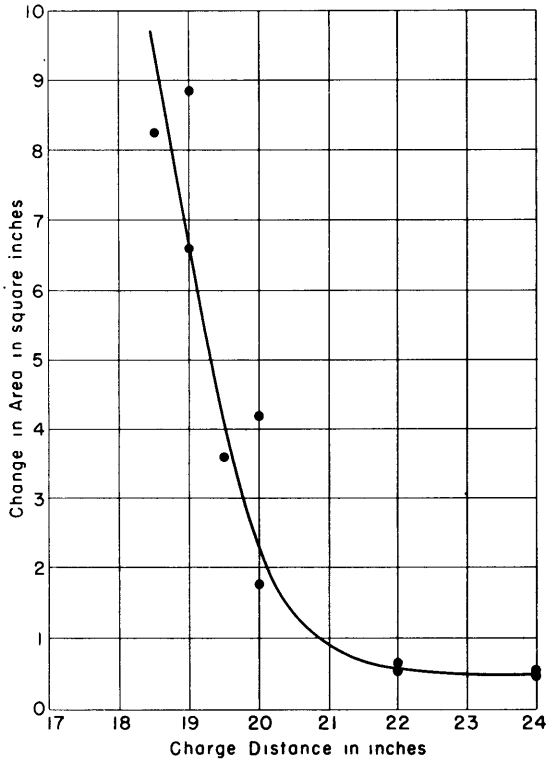

Figure 10 - Change in Area of Diaphragms plotted on Charge Distance

TEST RESULTS

The distances between the charges and each of the ten diaphragms are given in Table 1.

Diaphragms I-15, J-2, and J-8 split or ruptured. The ruptures of I-15 and J-2 were apparently due to the presence of the bearing weld at the center, since diaphragms J-5 and J-7, which did not have such a weld and were fired at the same distances from the charge, remained whole. On the other hand, diaphragm J-8 ruptured because of the nearness of the charge; this has been substantiated by experiments on other diaphragms not listed in this report.

From profiles drawn from the deformed diaphragms, it is possible to measure the total change in

TABLE 2

Final Change in Area of Diaphragms

Diaphragm	Charge Distance inches	Final Change in Area ΔA square inches
J-9	24.0	0.54
J-3	24.0	0.50
J-6	22.0	0.55
J-1	22.0	0.65
J-5	20.0	4.18
I-15 (R)*	20.0	1.77
J-10	19.5	3.59
J-7	19.0	6.60
J-2 (R)	19.0	8.85
J-8 (R)	18.5	8.25

* (R) indicates that the diaphragm was eventually ruptured.

area ΔA undergone by each diaphragm in deforming from a flat plate to its final shape. An approximate value for ΔA can be estimated in this way even for the ruptured diaphragms. These measurements are listed in Table 2 and plotted in Figure 10. They show a definite trend with distance. At larger

distances the change in area increases slightly as the charge distance decreases; then, as the distance becomes less than a certain critical distance between 20 and 22 inches there is a rapid increase in area which continues until the diaphragm ruptures. This trend has been reproduced several times under the conditions of this experiment in other series of 10-inch diaphragms.

Figure 10 also shows that there is some scattering* of the data around the smooth curve. The fluctuations seem to be due for some reason to the asymmetry of the setup; there is a target on only one side of the charge.

The high film speed of the camera necessarily stretches the streak records out so that it is difficult to visualize the overall motion of a spot. In order to gain a proper perspective of the motion, a slow-speed streak record of the motion was made and is included here in Figure 11.

The low-speed streak records of Figure 11 and the high-speed records of Figure 12 show an extremely high initial acceleration, evidenced by the sharp break in the slope of the streaks. Each diaphragm springs upward with a high initial velocity of the order of 1 inch per millisecond, while the barge eventually gains an upward velocity of roughly one-fifth of this amount. That the initial velocity acquired by the diaphragm is almost constant over the diameter may be seen by inspection of Table 3, in which the initial velocity measurements of the center spots are compared with the corresponding measurements on the spots midway between center and edge. The upward velocities acquired by the two balls on the edge of the mounting ring are also listed; the average of these two velocities could be taken as the velocity attained by

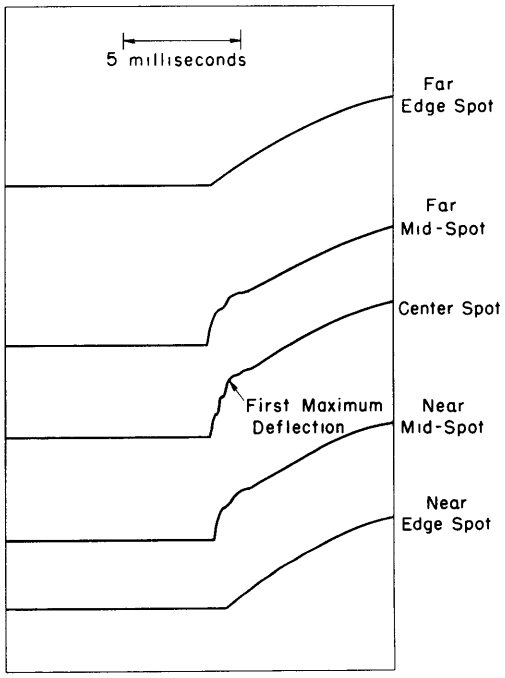

Figure 11 - An Enlarged Section of a Slow-Speed Streak Record

The record shows the motion of the diaphragm as it deforms out to its first maximum deflection.

* An independent investigation has been carried out to test the consistency of data obtained in explosion tests. The diaphragm and barge were completely submerged with the barge bottom and diaphragm in a vertical plane and with an air cavity on the opposite side of the diaphragm from the charge. The charge was at a fixed distance of 21 inches from the diaphragm, on the axis of the diaphragm and at a depth of 4 feet. Under these conditions, for 9 diaphragms, the average ΔA was 6.92 square inches, with a root mean square deviation of 15 per cent. Presumably the conditions of the experiment described in this report were such that similar large fluctuations in the change in area occurred.

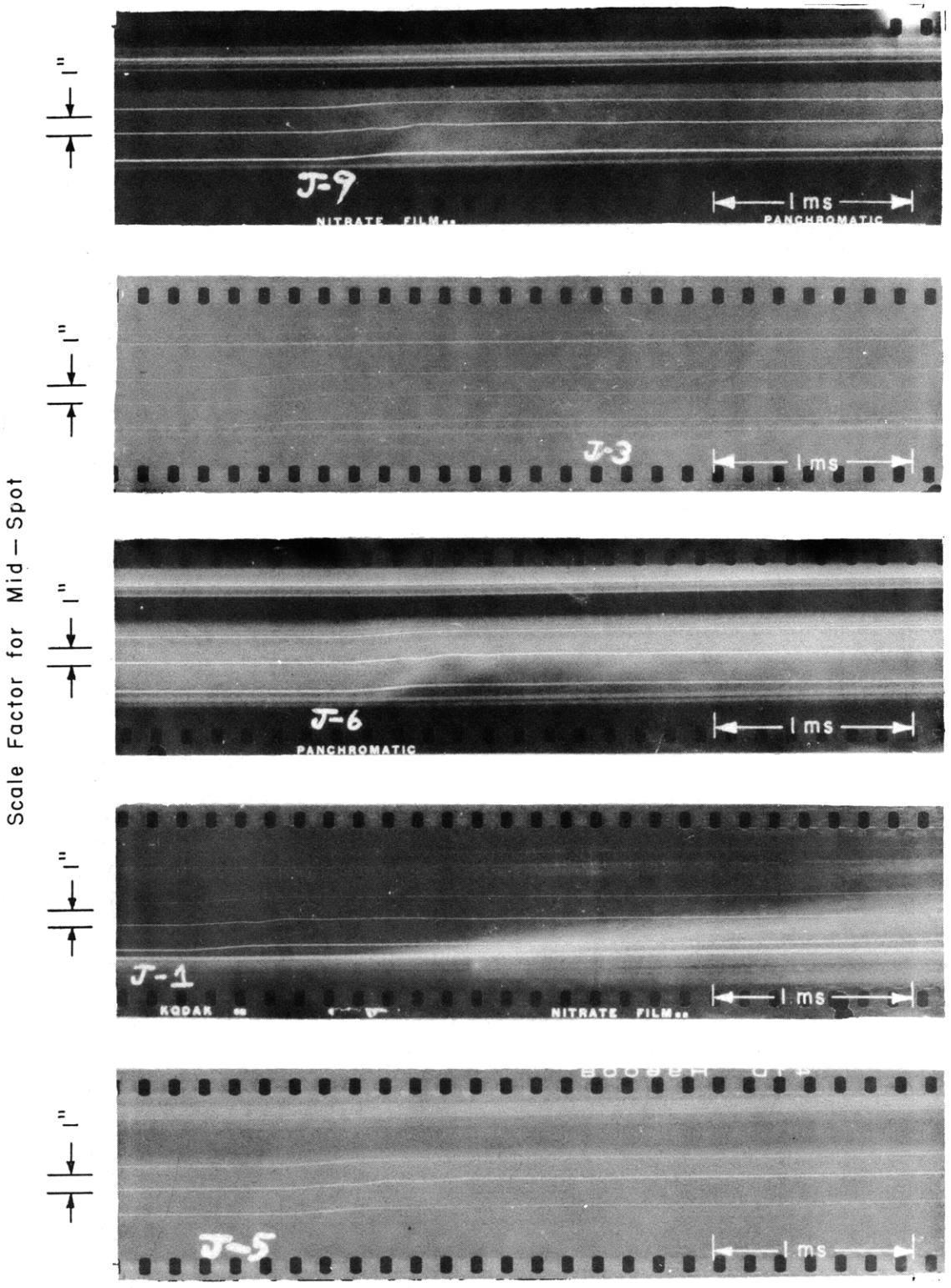

Figure 12 - Streak Photograph Records of Diaphragm Deformations

For the data derived from these records, see Tables 3 and 4 on pages 16 and 17.

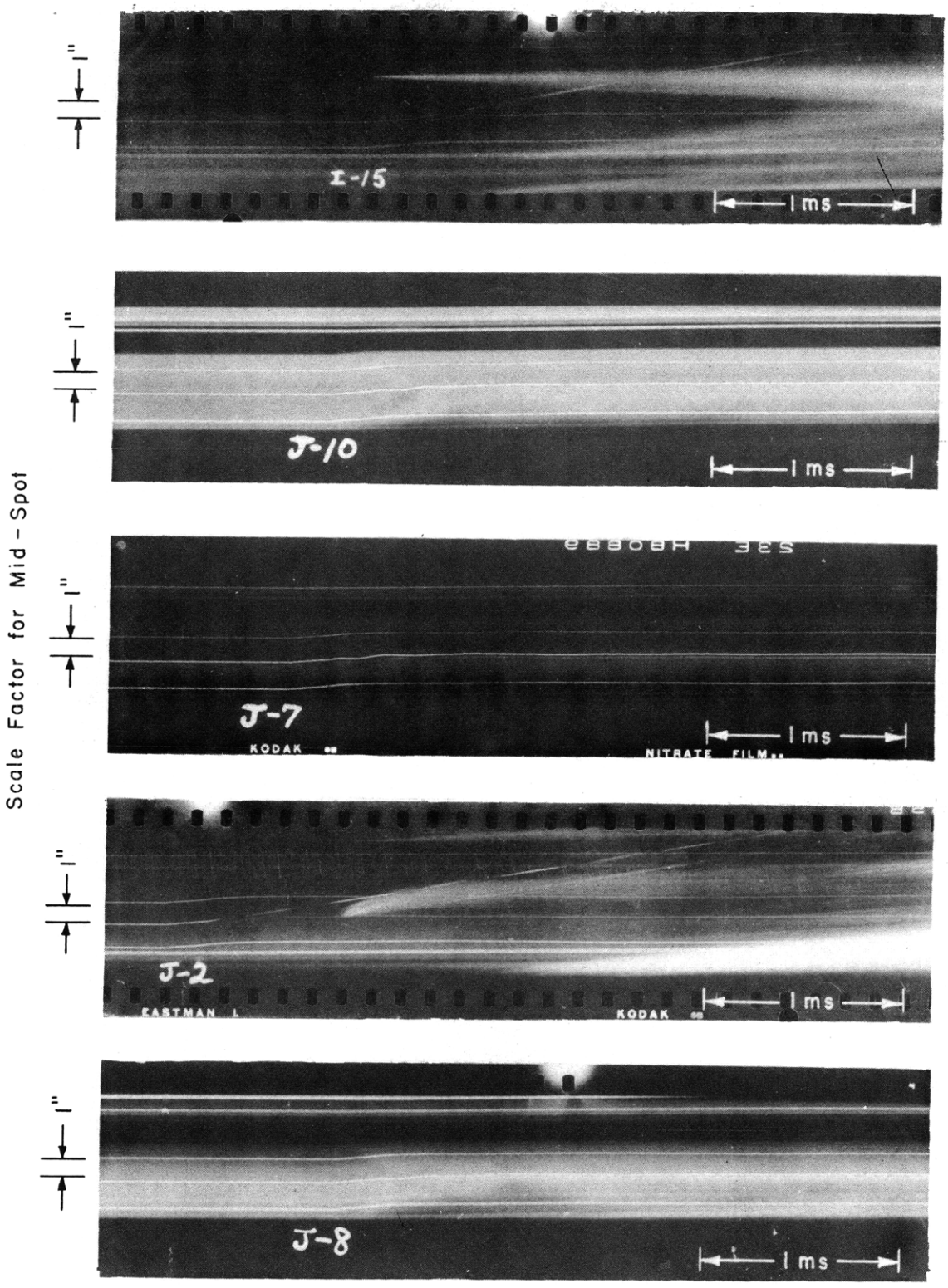

Figure 12 - Streak Photograph Records of Diaphragm Deformations.

For the data derived from these records, see Tables 3 and 4 on pages 16 and 17.

TABLE 3

Initial Velocities Acquired by Diaphragm and Mounting Rings

Diaphragm	Charge Distance inches	Velocity, inches per millisecond				
		Diaphragm			Mounting Ring	
		Center Spot	Far Mid-Spot	Near Mid-Spot	Far Edge	Near Edge
J-9	24.0	0.927	0.894	0.891	0.201	0.136
J-3	24.0	0.688	0.862	0.776	0.104	0.092
J-6	22.0	0.921	0.906	0.884	0.214	0.138
J-1	22.0	0.896	0.881	0.855	0.157	0.163
J-5	20.0	0.886	0.883	0.924	0.135	0.110
I-15 (R)*	20.0	0.932	1.051	0.911	0.206	0.167
J-10	19.5	1.031	1.036	1.097	0.152	0.183
J-7	19.0	1.089	1.090	1.104	0.225	0.231
J-2 (R)	19.0	1.019	1.046	1.014	0.142	0.157
J-8 (R)	18.5	1.110	1.050	1.068	0.205	0.215

* (R) indicates that the diaphragm was eventually ruptured.

the barge, if it were assumed that there are no vibrations of large amplitude of the bottom plate of the barge or the mounting ring. However, vibrations of this kind have recently been observed in tests to be described in a subsequent report. Consequently the average velocity referred to is simply the initial velocity of the central portion of the barge bottom.

A slight increase in the initial velocities of the diaphragms is noted as the charge distance is decreased.

Examination of the streak pictures of Figure 12 shows that all the diaphragms attain similar maximum deflections at about 1 millisecond from the initiation of the motion. After this deflection has been reached, the further motion of the diaphragms with respect to the mounting ring is quite small in the portions of the records shown. This small residual motion may be attributed to elastic spring-back of the diaphragms.

From measurements of the displacements at the center and mid-spots of the diaphragm relative to the mounting ring bearing balls, the changes in area of the diaphragms at any time may be estimated. Table 4 lists the values of increase in area at the time when the diaphragms have attained their first maximum displacements at about 1 millisecond.

The important feature of these measurements is the surprising discrepancy between these changes in area and the total changes in area measured

TABLE 4

Changes in Area of the Diaphragms Upon Reaching Their First Maximum Deflections

Diaphragm	Charge Distance inches	Estimated Change in Area at First Maximum Deflection, ΔA_1 square inches	Final Change** in Area ΔA square inches
J-9	24.0	0.301	0.54
J-3	24.0	0.445	0.50
J-6	22.0	0.301	0.55
J-1	22.0	0.310	0.65
J-5	20.0	0.485	4.18
I-15 (R)*	20.0	0.376	1.77
J-10	19.5	0.495	3.59
J-7	19.0	0.450	6.60
J-2 (R)	19.0	0.604	8.85
J-8 (R)	18.5	0.440	8.25

* (R) indicates that the diaphragm was eventually ruptured.

** From Table 2.

from the final profiles of the diaphragms. It may be observed that on the streak pictures of diaphragms I-15 and J-2 the center ball came off before the end of one millisecond. Hence the observation of the first maximum for these diaphragms is somewhat uncertain but can be estimated within perhaps 5 to 10 per cent from the streak record made by the bright weld spot under the bearing ball.

ANALYSIS OF THE TEST DATA

For convenience, Table 5 lists the constants used in obtaining the calculated results of this section.

As an approximation to the energy U_d absorbed by the diaphragm per unit area in reaching its final deformed state, the formula (3)

$$U_d = \sigma_y h \frac{\Delta A}{\pi a^2}$$

may be used where U_d is in inch-pounds per square inch and ΔA is the total increase in area in square inches. This formula is derived on the assumption that the stresses and strains are constant and uniform over the plate, and that the linear strain is equal to $\frac{1}{2}\frac{\Delta A}{\pi a^2}$. The values of U_d for the ten diaphragms are listed in Table 6.

TABLE 5

Constants Used in Calculations

Quantity	Symbol	Value	Units
Diaphragm radius	a	5	inches
Diaphragm thickness	h	0.0567	inches
Diaphragm density	ρ	0.283	pounds per cubic inch
Average yield stress*	σ_y	44×10^3	pounds per square inch
Young's modulus	E	30×10^6	pounds per square inch
Poisson's ratio	ν	0.3	
Charge weight	W	0.0484	pounds
Acceleration of gravity	g	386	inches per second squared

* This yield stress is taken from the customary static tensile tests. At present, tensile tests at high rates of loading are being conducted on this material, but results are not yet available.

TABLE 6

Observed Energy Values Calculated from Tables 2, 3, and 4
in Inch-Pounds per Square Inch

Diaphragm	Charge Distance inches	Energy of Final Damage U_d	Kinetic Energy of Initial Motion U_k	Plastic Work in the First millisecond U_{s1}
J-9	24.0	17.2	17.0	7.00
J-3	24.0	15.9	12.5	11.57
J-6	22.0	17.5	17.0	7.00
J-1	22.0	20.7	16.0	7.29
J-5	20.0	132.8	16.6	12.84
I-15	20.0	56.3	19.4	9.38
J-10	19.5	114.1	23.2	13.16
J-7	19.0	209.7	24.9	11.73
J-2	19.0	281.3	21.9	16.67
J-8	18.5	262.2	24.1	11.41

In Table 6 are also given the values of the initial kinetic energy per unit area, U_k. This is calculated from the formula

$$U_k = \frac{1}{2} \frac{\text{mass}}{\text{area}} \times \text{velocity squared} = \frac{1}{2} \frac{\rho h}{g} \bar{v}_d^{\,2}$$

where $\overline{v}_d$ is the average initial velocity over the diaphragm, taken from Table 3 as the average of the initial velocities of the center and mid-spots.

In order to calculate the work U_{s1} done on the diaphragm in swinging out to its first maximum deflection, consideration must be given to the fact that the diaphragm first deflects elastically and then plastically. An elementary estimate* shows that U_{s1} can be calculated from the formula

$$U_{s1} = \sigma_y h \frac{\Delta A_1}{\pi a^2} - 2.56$$

where ΔA_1 is the whole increase in area up to the first maximum. The values of U_{s1} so obtained are listed in Table 6 with the other calculated energies.

The curves of Figure 13 exhibit these results in graphic form.

Two striking observations are now made. First, in the range of charge distances less than a critical distance about 20 inches, the final damage done to the diaphragm, measured by U_d, is much greater than the work U_{s1} done on the diaphragm in the first millisecond. Second, throughout the

---

* Let us suppose that, at any instant in this process, the diaphragm is wholly either all elastic or all plastic. Then the work U_{s1} done on the diaphragm in reaching its first maximum deflection is the sum of two quantities. The first is the work U_e done under the elastic conditions which prevail until the instant at which plastic yield begins; the second is the work U_{d1} done as the diaphragm deforms plastically from the limit of the elastic state to the first maximum deflection.

It can be shown (3) that, under the assumption that the stresses and strains are uniform and constant over the diaphragm, U_e is given by

$$U_e = \frac{1}{2} \sigma_y h \frac{\Delta A_y}{\pi a^2}$$

where ΔA_y is the change in area at which plastic yield begins. Furthermore, U_{d1} can be estimated from the formula

$$U_{d1} = \sigma_y h \frac{\Delta A_1 - \Delta A_y}{\pi a^2}$$

Consequently, the work done on the diaphragm in reaching the first maximum deflection is

$$U_{s1} = U_e + U_{d1} = \sigma_y h \frac{\Delta A_1 - \frac{1}{2} \Delta A_y}{\pi a^2}$$

Now ΔA_y is simply obtained from Hooke's law for plane stress, assumed to hold up to the yield point,

$$\sigma_y = \frac{E}{1 - \nu} \left(\frac{1}{2} \frac{\Delta A_y}{\pi a^2} \right)$$

From these considerations, ΔA_y is found, for the diaphragms of this report, to be

$$\Delta A_y = 0.161 \text{ square inch}$$

Hence

$$U_{s1} = \sigma_y h \frac{\Delta A_1}{\pi a^2} - 2.56$$

as stated in the text.

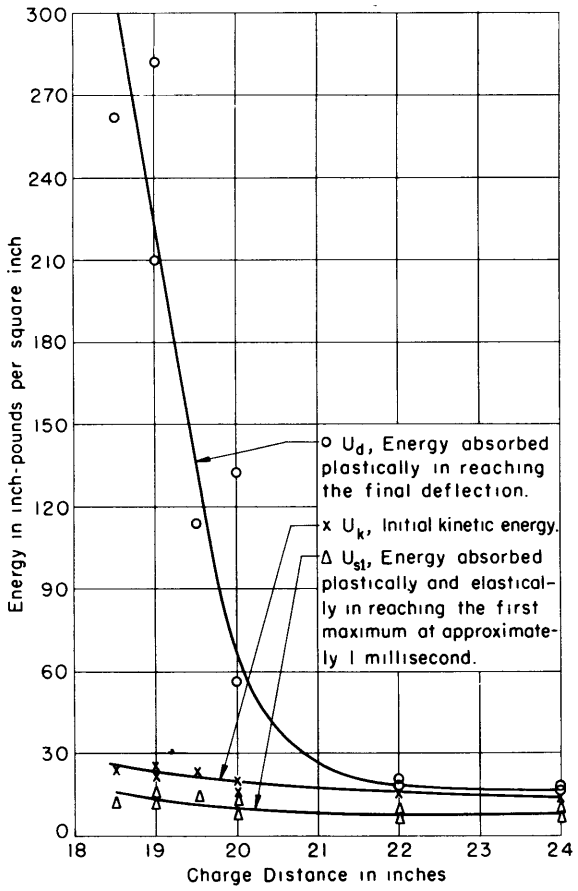

Figure 13 - Relation of Final to Initial Damages Plotted from Table 6

range of charge distances used, the work U_{s1} done on the diaphragm up to the first maximum deflection is on the average only 57 per cent of the value of the initial kinetic energy acquired by the diaphragm.

Concerning the first observation, it is to be emphasized that at the end of 1 millisecond the major portion of the initial shock wave, the A- and B-phases, has already done its damage. The only possible conclusion from this phenomenon is that there is some later action very effective in producing the final damage observed. This later action has been called the C-phase in the first part of this report.

It has been surmised that pressure pulses arising from subsequent compressions of the gas globe as it expands and contracts may account for the increased damage produced under these conditions. If the gas globe is attracted upward by the bottom of the barge as the gas globe compresses, the later pressure pulses can reasonably be expected to be more effective in producing damage than the A- and B-phases due to the proximity of the gas globe to the diaphragm.

This hypothesis may account for the observed critical distance. The steepness of the rise in the final damage curve of Figure 13, as the charge distance decreases, might suggest some sort of resonance phenomenon. That is, the frequency of the globe oscillations, in the range from 8 to 25 cycles per second for this size charge, may nearly equal some natural frequency of the structure.* So far, however, no such natural frequency of the structure has been discovered.

The second observation leads necessarily to the conclusion that part of the initial kinetic energy must have gone into work done elsewhere

* One natural frequency of the barge bottom plate is about 66 cycles per second.

than on the diaphragm. Moreover, if there are hydrodynamic pressures acting during the first upward swing, these also must do work on the diaphragm. Consequently, possibly *more* than 43 per cent on the average of the initial kinetic energy imparted by the shock wave to the diaphragm must be dissipated elsewhere and not manifest itself in work done on the diaphragm.

ENERGY DISSIPATION

What becomes of the part of the initial kinetic energy which does not go into damage? Rough estimates may be obtained from the following considerations. In deflecting upward, the diaphragm exerts a pull on the mounting and holding rings. This force is the resultant of the vertical component of the tension $\sigma_y h$ at the edge of the diaphragm.

The fact that the velocity of the diaphragm as it bulges upward is initially almost constant over its central portion points to a type of motion illustrated in Figure 14. This kind of motion suggests that the slope $\left(\frac{\partial z}{\partial r}\right)_{r=a}$ at the edge of the diaphragm remains practically constant during the deflection. Hence, if ΔZ_{e1} is the displacement of the mounting ring when the diaphragm reaches its first maximum deflection, the work done per unit area of diaphragm on the mounting ring is approximately

$$U_{w1} = 2\pi a \sigma_y h \left(\frac{\partial z}{\partial r}\right)_{1(r=a)} \frac{\Delta Z_{e1}}{\pi a^2}$$

This is one source of loss of energy in the first millisecond.

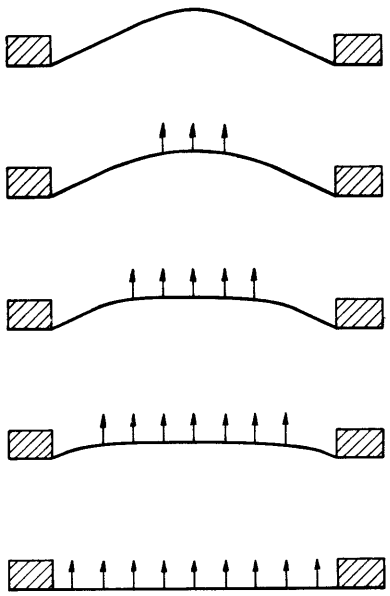

Figure 14 - Motion of the Diaphragm Inferred from the Streak Photographs

The time scale reads from the bottom upward. The arrows indicate motion of the diaphragm.

Another possibility arises if we grant the assumption of cavitation just after the impact of the initial shock front. Then the pressure below the diaphragm is practically zero, so that the diaphragm does work against the atmospheric pressure p_0. The work per unit area done in the first millisecond is

$$U_{a1} = p_0 \frac{V_1}{\pi a^2}$$

where V_1 is the volume swept out by the diaphragm in deflecting. Table 7 compares the energies U_{w1} and U_{a1} estimated in this way with the diaphragm's

TABLE 7

Estimated Energy Values Calculated from Data in Tables 2, 3, and 4 in Inch-Pounds per Square Inch

Diaphragm	Charge Distance inches	U_k	U_{s1}	U_{w1}	U_{a1}	U_1
J-9	24.0	17.0	7.00	6.91	2.60	16.5
J-3	24.0	12.5	11.57	7.10	3.32	22.0
J-6	22.0	17.0	7.00	8.21	2.67	17.9
J-1	22.0	16.0	7.29	7.02	2.80	17.1
J-5	20.0	16.6	12.84	4.43	3.46	20.7
I-15	20.0	19.4	9.38	9.59	2.82	21.8
J-10	19.5	23.2	13.16	8.66	3.39	25.2
J-7	19.0	24.9	17.73	10.57	3.14	31.4
J-2	19.0	21.9	16.67	9.47	3.54	29.7
J-8	18.5	24.1	11.41	7.98	3.29	22.7

U_{a1} is the work done against atmospheric pressure in the cavitation phase. The slope $\left(\frac{\partial z}{\partial r}\right)_{r=a}$ and the volume V_1 used to calculate these quantities are estimated from the diaphragm profiles obtained from the streak photographs at the first maximum deflections. The column headed U_1 represents the sum of U_{s1}, U_{w1} and U_{a1}; that is, it represents the total estimated energy dissipated by the diaphragm in its bulge upward to the first maximum. It is roughly equal to U_k.

initial kinetic energy and the elastic and plastic work done on it in the first bulge upward.

In Figure 15 there are plotted the curves of U_k, U_{s1}, and U_1 on a basis of charge distance, from which it may be noted that the total energy dissipated in the first upward deflection is very nearly equal to the initial kinetic energy of the diaphragm.

This is a satisfying but slightly uncertain result because of the crudeness of the estimations. However, the small systematic difference between the U_k and U_1 curves show that little work is done by the pressures of the B-phase. Although this difference is of the order of the uncertainty in the approximations, it may be said that here is evidence for the relative ineffectiveness of the B-phase in producing damage.

In this study of the energy relations, possible effects arising from the relative motion of the water and the diaphragm have been ignored. If cavitation does not occur, the water must be moving with the diaphragm, with a consequent addition in initial kinetic energy to that of the diaphragm.

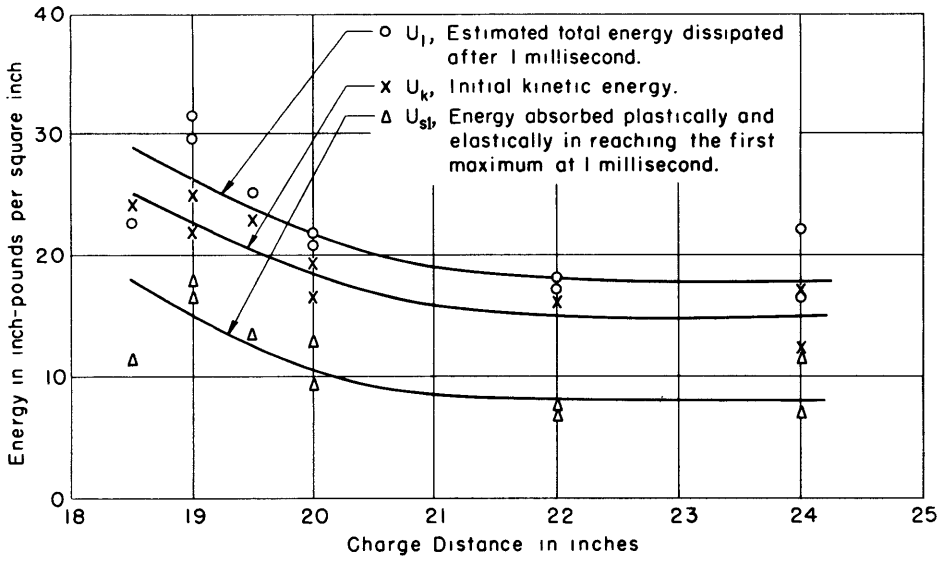

Figure 15 - Variation of Initial Energies with Distance

These curves are plotted from values in Table 7.

If, as seems much more probable, cavitation does occur, either under the whole diaphragm or under part of it, the water should follow the diaphragm and eventually overtake it and press upon it; evidence for this action may lie in the strange oscillation of the center spot on the diaphragm, as seen in Figures 11 and 12. It is interesting to note in this connection that cavitation has been observed to occur at the center of a plastic window surrounding a submerged light source and exposed to an underwater explosion.

Two forces may accelerate the water toward the diaphragm. The hydrostatic pressure, if not resisted by the under surface of the diaphragm, will act on the water and accelerate it. Diffraction of the incident shock wave from surrounding regions may also contribute to the acceleration of the water, although this action may be greatly reduced by the occurrence of cavitation under the barge itself.

THE SOLID ANGLE LAW

One further investigation is suggested by the data at hand. Because of spherical symmetry, the energy carried by the shock wave in any solid angle subtended at the charge remains constant. Consequently, if a constant proportion of the shock wave energy is imparted initially to the diaphragm as kinetic energy, this kinetic energy should vary as the solid angle $\overline{\omega}$, subtended by the diaphragms at the charge (4). The number F_i, which may be called the initial field coefficient (4), and is defined as the initial kinetic energy imparted to the diaphragm per unit weight of charge and per unit solid angle, should be a constant for the ten diaphragms.

TABLE 8

Initial Field Coefficient*

Diaphragm	Charge Distance inches	$F_i \times 10^{-3}$ inch-pounds per pound charge per unit solid angle
J-9	24.0	207
J-3	24.0	152
J-6	22.0	177
J-1	22.0	166
J-5	20.0	142
I-15	20.0	166
J-10	19.5	191
J-7	19.0	194
J-2	19.0	171
J-8	18.5	180

* The initial field coefficient is the initial kinetic energy per unit charge weight per unit solid angle.

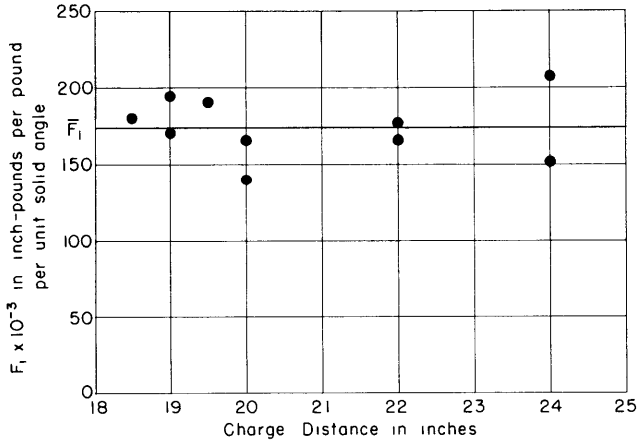

Figure 16 - Variation of Initial Field Coefficient with Charge Distance, Plotted from Table 8

Table 8 gives the result of calculating F_i for each of the ten diaphragms. These values are plotted in Figure 16 on a basis of charge distance. Although the dispersion is rather large, there is no observable dependence of F_i on charge distance. The mean value of F_i from these data is

$$\overline{F}_i = (175 \pm 19) \times 10^3 \text{ inch-pounds per pound per unit solid angle}$$

with an indicated RMS deviation from the mean of about 11 per cent.

CONCLUSIONS

Under the conditions and circumstances described in this report, we may state the following:

(a) Most of the damage done by an underwater explosion to a thin circular diaphragm, at less than a critical distance, occurs *after* the initial shock wave has ceased to act. This is evidence for the effectiveness of the C-phase in producing damage.

(b) At about 1.5 millisecond for a 22.7 gram charge, after which time both the A- and B-phase of the shock wave have passed, the damage to the diaphragm is less than if all the kinetic energy initially acquired had been expended in damaging the diaphragm. This is evidence against the effectiveness of the B-phase in causing damage.

(c) In the moderate range of charge distances investigated here the initial kinetic energy imparted by the initial shock wave to the target is roughly proportional to the solid angle subtended by the target at the charge.

The magnitudes of these effects for charges and diaphragms of different sizes have not yet been investigated. Experiments along these lines, together with an extension of the observations to larger ranges of charge distances, are planned for the immediate future.

REFERENCES

(1) "The Vertical Motion of a Spherical Bubble and the Pressure Surrounding It," by Professor G.I. Taylor, F.R.S., TMB CONFIDENTIAL Report 510, August 1943.

(2) "Photographic Methods of Recording Behavior of Steel Diaphragms under Explosive Load," by Dr. D. Bancroft and Dr. B.L. Miller, TMB CONFIDENTIAL Report R-66, August 1942.

(3) "Protection Against Underwater Explosion, Plastic Deformation of a Circular Plate," by Dr. A.N. Gleyzal, TMB Report 490, September 1942.

(4) "The Design of Ship Structure to Resist Underwater Explosion, Nominal Theory," by Captain W.P. Roop, USN, TMB CONFIDENTIAL Report 492, July 1943.